



# Mathematical Modeling of 3D Tissue Engineering Constructs

Henrique Amorim Almeida and Paulo Jorge da Silva Bártolo

## Contents

1	Introduction .....	224
2	Mathematical-Based Scaffold Modeling .....	225
3	Triply Periodic Minimal Surfaces .....	231
3.1	Definition .....	231
3.2	Periodic Surface Modeling .....	232
3.3	Schwarz TPMS Primitives .....	234
3.4	Schoen TPMS Primitives .....	235
4	Numerical Implementation of the Designed Models .....	237
4.1	Elastic Modulus Evaluation .....	238
4.2	Shear Modulus Evaluation .....	244
5	Design of a Functionally Gradient Scaffold Using TPMS Basic Units .....	245
6	Conclusions .....	246
	References .....	249

## Abstract

Tissue engineering represents a new field aiming at developing biological substitutes to restore, maintain, or improve tissue functions. In this approach, scaffolds provide a temporary mechanical and vascular support for tissue regeneration while tissue ingrowth is being formed. The design of optimized scaffolds for tissue engineering applications is a key topic of research, as the complex

---

H. A. Almeida (✉)

School of Technology and Management, Polytechnic Institute of Leiria (IPL), Leiria, Portugal  
e-mail: [henrique.almeida@ipleiria.pt](mailto:henrique.almeida@ipleiria.pt)

P. J. da Silva Bártolo

Manchester Biomanufacturing Centre, University of Manchester, Manchester, UK

School of Mechanical, Aerospace and Civil Engineering, University of Manchester, Manchester, UK

e-mail: [paulojorge.dasilvabartolo@manchester.ac.uk](mailto:paulojorge.dasilvabartolo@manchester.ac.uk)

macro- and micro-architectures required for a scaffold depends on the mechanical and vascular properties and physical and molecular queues of the surrounding tissue at the defect site. One way to achieve such hierarchical designs is to create a library of unit cells, which can be assembled through a computational tool.

Besides presenting an overview scaffold designs based hyperbolic surfaces, this chapter investigates the use of two different types of triply periodic minimal surfaces, Schwarz and Schoen, in order to design better biomimetic scaffolds with high surface-to-volume ratio, high porosity, and good mechanical properties. The effect of two parametric parameters (thickness and surface radius) is also evaluated regarding its porosity and mechanical behavior.

---

## 1 Introduction

The loss or failure of an organ or tissue is a frequent, devastating, and costly problem in health care. Currently, this problem is treated either by transplanting organs from one individual to another or performing surgical reconstructions, transferring tissue from one location in the human body into the diseased site. With the aging of the population and higher expectations for a better quality of life, the need for substitutes to replace or repair tissues or organs due to disease, trauma, or congenital problems is overwhelming and increasing on a daily basis. To overcome these limitations, tissue engineering emerged as a rapidly expanding approach to address the organ shortage problem by creating cell-based substitutes of native tissues comprising tissue regeneration, organ substitution, and gene therapy (Melek 2015; Risbud 2001; Langer and Vacanti 1993).

Tissue engineering is a multidisciplinary field focusing on the use of cells and engineered materials, combining the principles of biology, engineering, and medicine to create biological substitutes for lost or defective native tissues (Jiang et al. 2015; Eshraghi and Das 2010; Bártolo et al. 2008, 2009a, b; Gibson 2005; Tan et al. 2005; Vozzi et al. 2003; Risbud 2001). According to Skalak and Fox (1988), tissue engineering is defined as “the application of the principles and methods of engineering and life sciences toward the fundamental understanding of structure–function relationships in normal and pathological mammalian tissues and the development of biological substitutes to restore, maintain, or improve tissue and organ functions” (Jiang et al. 2015; Bártolo et al. 2008).

In tissue engineering applications, a temporary three-dimensional scaffold that mimics the physiological functions of the native extracellular matrix is vital to stimulate and maintain the cells’ ability to express their native differentiated phenotypes. An optimal scaffold design can promote cell proliferation and cell-specific matrix production, which will eventually take over the supporting role of the biodegrading scaffold in situ (Xue et al. 2017; Fallahiarezoudar et al. 2015; Janik and Marzec 2015; Osman et al. 2015; Selimis et al. 2015; Bártolo et al. 2009a, 2009b).

To achieve these goals, an ideal scaffold must satisfy some biological and physical requirements (Tajbakhsh and Hajiali 2017; Law et al. 2016; Brunello et al. 2016; Tollemar et al. 2016; Stratton et al. 2016; Jana and Lerman 2015; Almeida and Bártolo 2012a, b). The biological requirements are biocompatibility (the scaffold material must interact positively with the cells, allowing cell attachment, proliferation, differentiation and with the host environment, without eliciting adverse host/tissue responses), biodegradability (the scaffold material must degrade into nontoxic products), controlled degradation rate (the degradation rate of the scaffold must be adjustable in order to match the rate of tissue regeneration), and bioactivity (promoting and guiding cell proliferation, differentiation, and tissue growth). The physical requirements are appropriate porosity, pore size and pore shape to encourage tissue ingrowth and vascularization, sufficient strength and stiffness to withstand stresses in the host tissue environment, adequate surface finish to ensure a good biomechanical coupling between the scaffold and the tissue, and easily sterilized by either exposure to high temperatures or immersing in a sterilization agent, remaining unaffected by neither of these processes.

Alongside the listed biological and physical requirements, an optimum scaffold should also have functional and anatomical requirements, in other words, a gradient functionality of the organ or tissue, meaning that the external geometry and size of the scaffold should be the same of the natural tissue, in order for the scaffold to fit and anchor onto the defected location. By applying these design concepts, a better fixation can be achieved by the scaffold, while facilitating better stress distribution in the interface between the surrounding tissue and the scaffold (Jazayeri et al. 2017; Giannitelli et al. 2015; Bártolo et al. 2012).

Several research works developed methodologies to control the topological architecture of scaffolds, aiming at obtaining better biological and mechanical properties and scaffold performance (Almeida et al. 2007a, b). As a result, several libraries and computational systems have been developed and applied for optimal scaffold design (Almeida and Bártolo 2008). This chapter gives an overview of mathematical design methodologies that have been applied to optimize scaffold design, namely, periodic-based geometric modeling approaches.

---

## 2 Mathematical-Based Scaffold Modeling

Most works on scaffold design for tissue engineering applications are either based on lattice structures with straight edges and sharp corners or in shapes obtained through Boolean operations with geometric primitives. Recently, hyperbolic surfaces, namely, triply periodic minimal surface (TPMS), have received increasing attention, as they enable the design of biomimetic scaffolds allowing the design of scaffolds with very high surface-to-area ratios, enhancing cell proliferation and cell-cell interactions, maximizing both porosity and mechanical performance (Qi and Wang 2009; Jung et al. 2007; Wang 2007; Gandy et al. 2001; Nesper and Leoni 2001; Hyde and Oguey 2000).

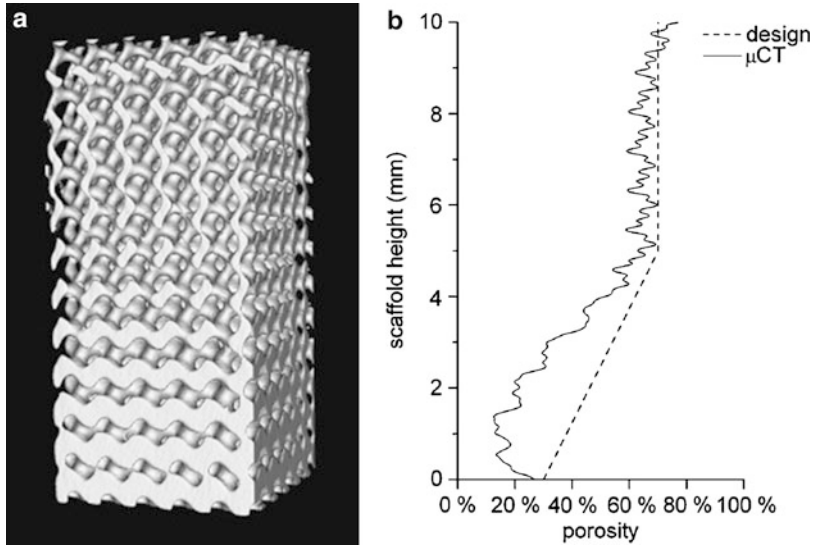


**Fig. 1** Built PDLLA scaffold with gyroid architecture showing a gradient in porosity and pore size. (a):  $\mu$ CT visualization. (b): Change in the average porosity with scaffold height (solid line) in comparison with the designed porosity (dotted line) (Melchels et al. 2010b)

Rajagopalan and Robb (2006) obtained results in the first effort regarding computer-controlled fabrication, modulation, and mechanical characterization of tissue engineering scaffolds based on TPMS. They designed simple cube models of P-scaffolds and manufactured them with a layer-based fabrication device. They also presented novel strategies to realize coterminous seeding-feeding networks, thereby assuring blood/nutrient supply to the proliferating cells at close proximity with the proposed geometries. The work provided insights on the reason behind the natural choice of TPMS forms in biological systems, by performing uniaxial and bulk compressive simulation using the finite element code.

Melchels et al. (2010b) used the K3DSurf software to generate scaffolds based on gyroid (G) and diamond (D) architectures. The gradient in pore size and porosity of the gyroid structure was introduced by adding a linear term to the equation for z-values (Fig. 1). They also demonstrated that, in the gyroid architectures, stress and strain are much more homogeneously distributed throughout the structure than for regular cubic architectures. A tissue engineering scaffold with gyroid architecture will expose adhering cells to a more equal mechanical stimuli throughout the structure. As cells respond to the deformation of the matrix to which they adhere (Bao and Suresh 2003), these structures present optimum mechanobiological stimulation.

Melchels et al. (2010a) assessed the influence of scaffold pore architecture on cell seeding and static culturing, by comparing a computer-designed gyroid architecture fabricated by stereolithography with a random pore architecture resulting from salt leaching. The scaffold structures showed comparable porosity and pore size values,

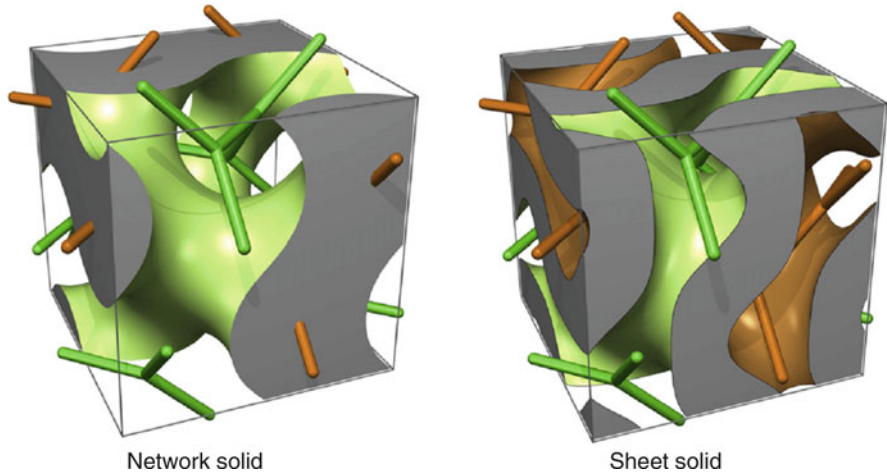


**Fig. 2** Scaffold designs of 50% volume fraction derived from the gyroid minimal surface. *Left:* Network solid architecture. The minimal surface partitions space into two interwoven domains. One is filled with an isotropic elastic material, the other is left empty (void domain). *Right:* Sheet solid architecture: The solid domain is given by a sheet of thickness  $r$ , folded onto the gyroid minimal surface. The value of  $r$  is adjusted to yield a volume fraction of 50% (Kapfer et al. 2011)

but the gyroid type showed a 10-fold higher permeability, due to the absence of size-limiting pore interconnections. The results also demonstrated that it is possible to control the cell seeding upon the scaffold with the geometric gyroid variation within the scaffold.

Yoo (2011a) presented a computer-aided porous scaffold design method based on TPMS. In this work, Yoo proposed a novel method for extracting surface and solid models directly from the approximated implicit surfaces for TPMS, based on the periodic surface model. The TPMS were described with periodic surfaces, composed of simple trigonometric functions, thus enabling easy generation of TPMS for use in various mechanical, chemical, and physical applications. A new control approach for pore size distribution was also presented, based on the pore-making element composed of TPMS, and conformal refinement of all hexahedral mesh, showing the practical applicability of the newly suggested modeling approach. The proposed modeling method was successfully validated through many designs of bone scaffold models.

Kapfer et al. (2011) observed that two types of scaffold architectures can be generated using TPMS-based unit cell libraries (Fig. 2). In this work, two types of solids based on minimal surface network solids and minimal surface sheet solids were designed. They showed that, for the same solid volume fraction, sheet solids have a substantially higher effective bulk modulus and direction-averaged Young's modulus than network solids, for a wide range of volume fractions and material parameters. The sheet solids also present a larger surface area for cell adhesion and proliferation.

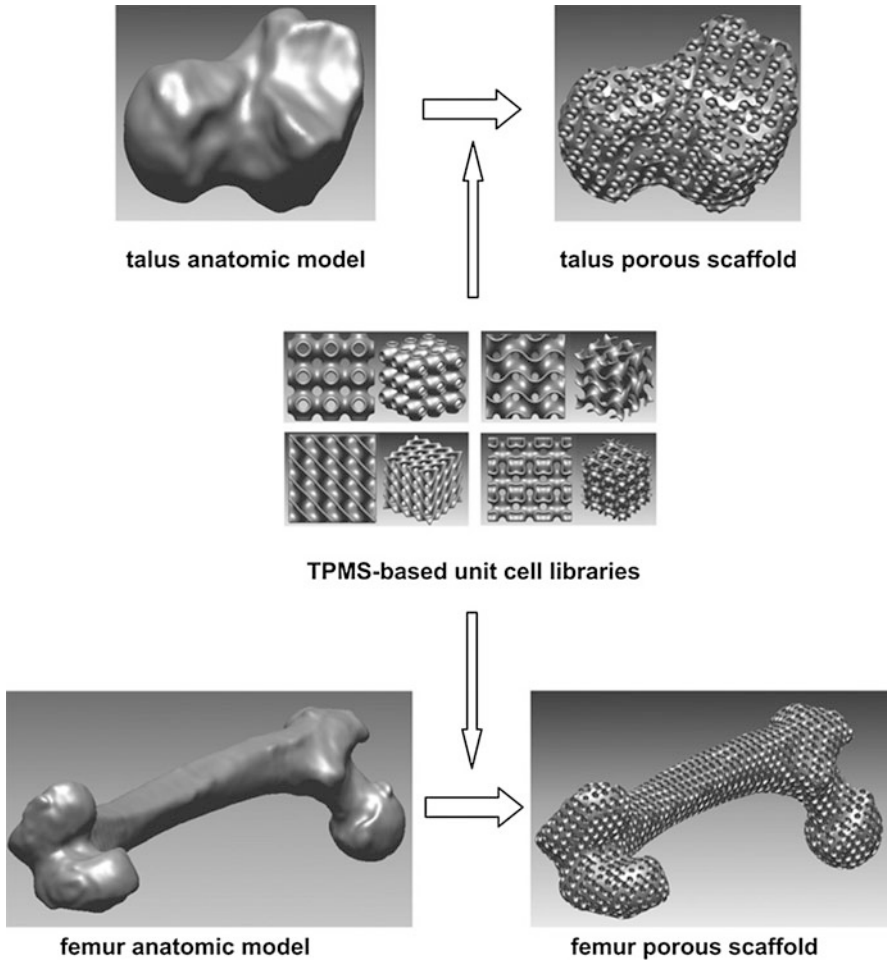


**Fig. 3** Porous scaffolds designed with intricate internal architectures and high-quality external surfaces (Yoo 2011b)

Yoo (2011b) proposed an effective method for the design of 3D porous scaffolds, based on a hybrid method of distance field and TPMS. By the creative application of a traditional distance field algorithm into the Boolean operations of the anatomical model and TPMS-based unit cell library, an almost defects' free porous scaffolds with a complicated microstructure and high-quality external surface, faithful to a specific anatomic model, can be easily obtained without difficult and time-consuming trimming and re-meshing processes. Figure 3 illustrates the Boolean operations between the anatomic models and TPMS-based unit cell libraries.

Yoo (2012a) proposed a heterogeneous porous scaffold design scheme, which is a direct extension of the control approach for pore size distribution in a previous work (Yoo 2011a). In this work, he proposes a novel heterogeneous modeling

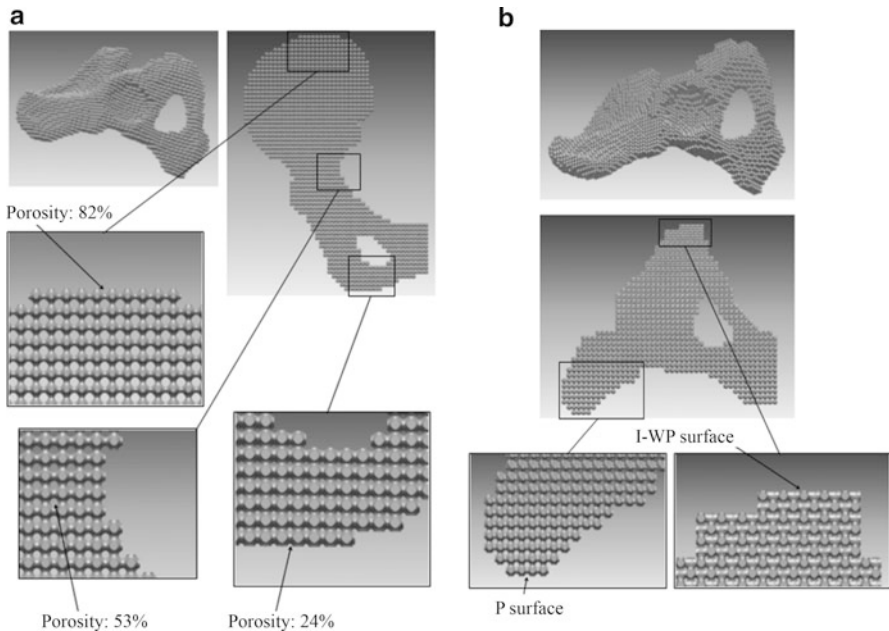


**Fig. 4** (a) Heterogeneous iliac scaffold design with controlled porosity. (b) Heterogeneous iliac scaffold design with controlled internal architectures (Yoo 2012a)

methodology for designing tissue engineering scaffolds, with precisely controlled porosity and internal architectures using TPMS. The major contribution of this work was to extend the range of heterogeneity, from the porosity only, to the combination of porosity and internal architecture type. In addition, by introducing a fourth scalar value at the nodes of eight-node hexahedral element related to the porosity and internal architecture type, he could determine the internal architecture type and porosity at the spatial locations, uniquely and continuously within arbitrary and complex 3D anatomical shapes. Another advantage of the proposed method is the possibility to control the pore size distribution without changing the size of hexahedral element, while maintaining perfectly interconnected pore networks. Figure 4 illustrates a heterogeneous iliac scaffold design showing either a controlled porosity or internal architecture.

Yoo (2012b) presented a general design framework for 3D internal scaffold architectures to match desired mechanical properties and porosity simultaneously, by introducing an implicit interpolation algorithm based on the radial basis function (RBF) (Fig. 5). Similarly to his previous work, the work focused on the computational heterogeneous tissue engineering scaffold design. While using all the strategies developed in previous works, such as Boolean operations based on the distance field and internal architecture construction using the TPMS-based unit cell libraries, special emphasis was given to an automated porosity distribution control algorithm based on the RBF. With the developed computer program, he demonstrated that the

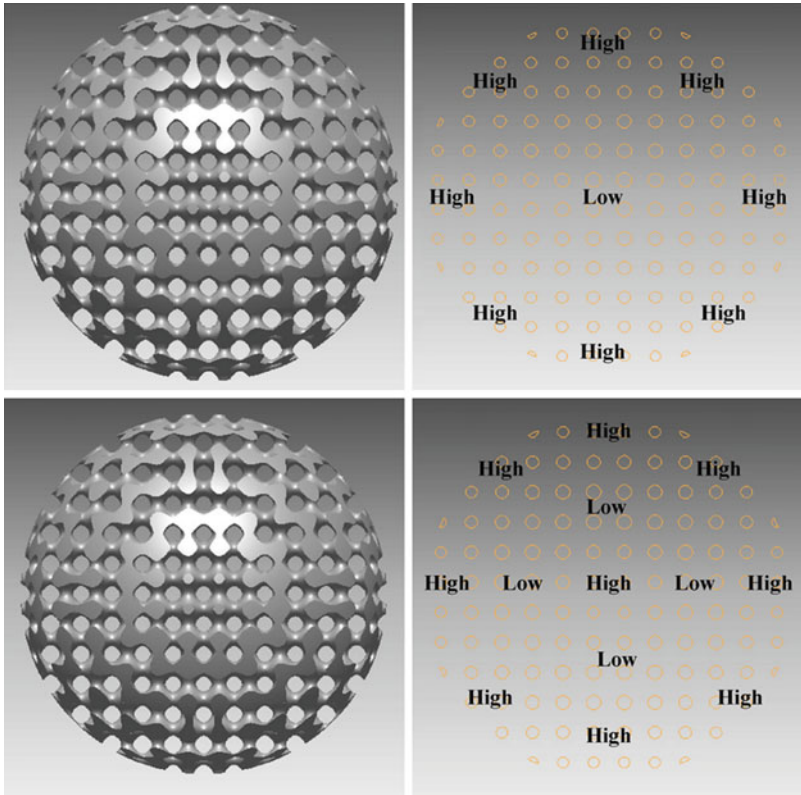


**Fig. 5** Heterogeneous sphere-shaped scaffolds having P-surface internal architectures with various gradients in porosity in the radial direction (Adapted from Yoo 2012b)

method can produce highly porous and heterogeneous structures matching the required anisotropic stiffness, using a set of porosity levels defined at some points selected by the user. In a later work, Yoo (2013) developed a hybrid method which combines radial basis functions with the TPMS transformation strategy. Experimental results show that the proposed scaffold design method is capable of controlling the internal pore architectures within an arbitrarily shaped scaffold while preserving the advantages of the distance field and TPMS-based pore architectures as illustrated in Fig. 6.

Yoo (2014) developed another design concept of multi-void TPMS-based scaffolds that increase the surface area to volume ratios of conventional TPMS scaffolds. Yoo suggests that the proposed novel design methodology can be applied to create a variety of design models for biomimetic scaffolds and bioartificial tissues. Figure 7 illustrates the multi-void design algorithm that was implemented for the scaffold design.

Dinis et al. (2014) developed an open source software tool for the design of scaffolds (Fig. 8). With the aid of the developed software and its geometric database

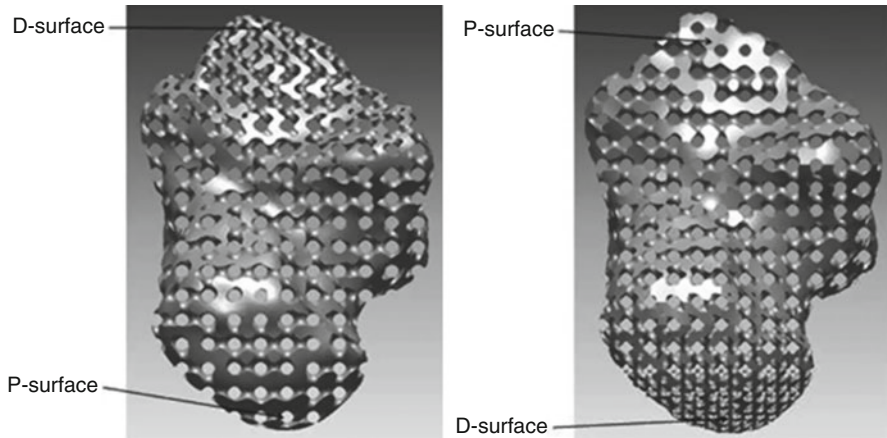


**Fig. 6** Heterogeneous talus bone porous scaffolds with continuous gradients in pore architectures between D-surface and P-surface (Adapted from Yoo 2013)

based on TPMS, different highly complex geometric models with different levels of porosity and permeability can be obtained. Based on the results, it is possible to observe that with the same construction parameters, the Neovius present the highest levels of porosity followed by the Gyroid, Schwartz\_P, Schwartz\_D, and (IWP) respectively.

### 3 Triply Periodic Minimal Surfaces

#### 3.1 Definition

In the 1880s, Schwarz described the first periodic minimal surface (Dinis et al. 2014). A minimal surface is a surface that is locally area minimizing, in other words, a small piece presents the smallest possible area of a surface spanning the boundary of that same piece. The surfaces were generated using symmetry arguments: given a solution to a Plateau's problem for a polygon, and the reflections of the surface across the boundary lines also produce valid minimal surfaces that can be continuously joined to the original solution (Dinis et al. 2014; Karcher and Polthier 2014). Among the various hyperbolic surfaces, the minimal surfaces are the most studied. If a minimal surface presents a space group symmetry, it is both infinite and periodic in three independent directions; therefore, it is called triply periodic minimal surface (TPMS). Another geometric characteristic of TPMS is that they present a mean curvature of zero. Examples of TPMS are illustrated in Fig. 9 (Kapfer et al. 2011).

Triply periodic minimal surfaces are also considered biomimetic surfaces as they commonly exist in natural structures, such as lyotropic liquid crystals, zeolite sodalite crystal structures, diblock polymers, hyperbolic membranes (prolamellar structure of chloroplasts in plants), echinoderm plates (interface between the

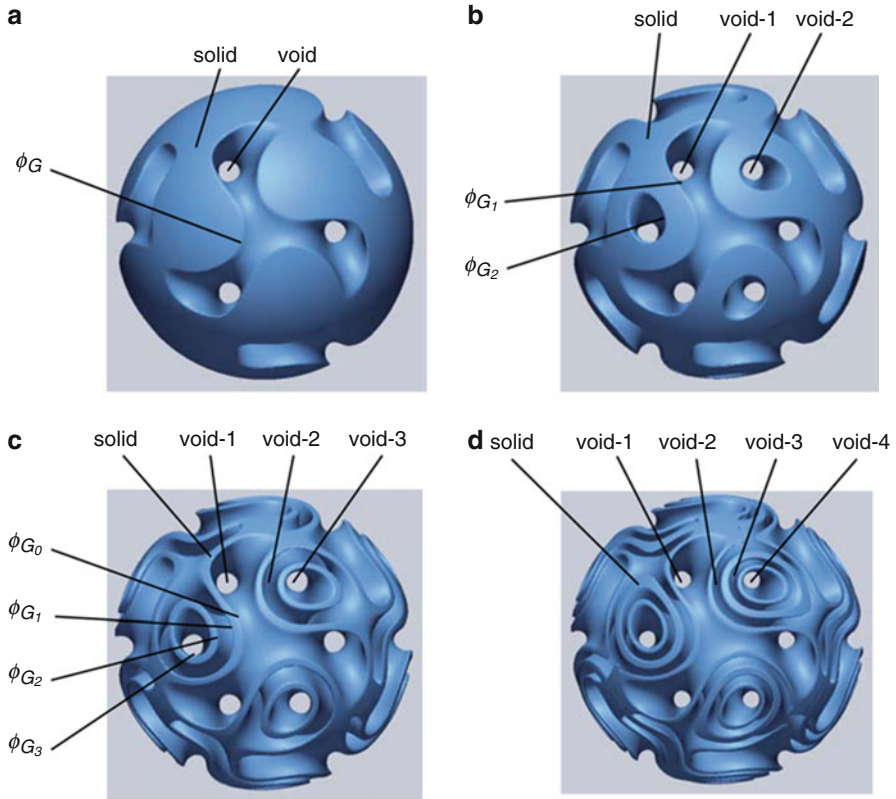


**Fig. 7** A sphere-shaped scaffold model with: (a) 1 void, (b) 2 voids, (c) 3 voids, and (d) 4 voids (Yoo 2014)

inorganic crystalline and organic amorphous matter in the skeleton), cubosomes and certain cell membranes (Dinis et al. 2014; Karcher and Polthier 2014; Almeida and Bártolo 2012a, b; Larsson et al. 2003; Sun and Lal 2002; Hyde 1996; Andersson 1983; Scriven 1976).

### 3.2 Periodic Surface Modeling

A periodic surface can be defined by the following mathematical model (Wang 2007; Rajagopalan and Robb 2006; Lord and Mackay 2003; Andersson et al. 1988):

$$\varphi(r) = \sum_{k=1}^K M_k \cos [2\pi (\mathbf{L}_k \cdot r) / \beta_k + P s_k] = C \quad (1)$$

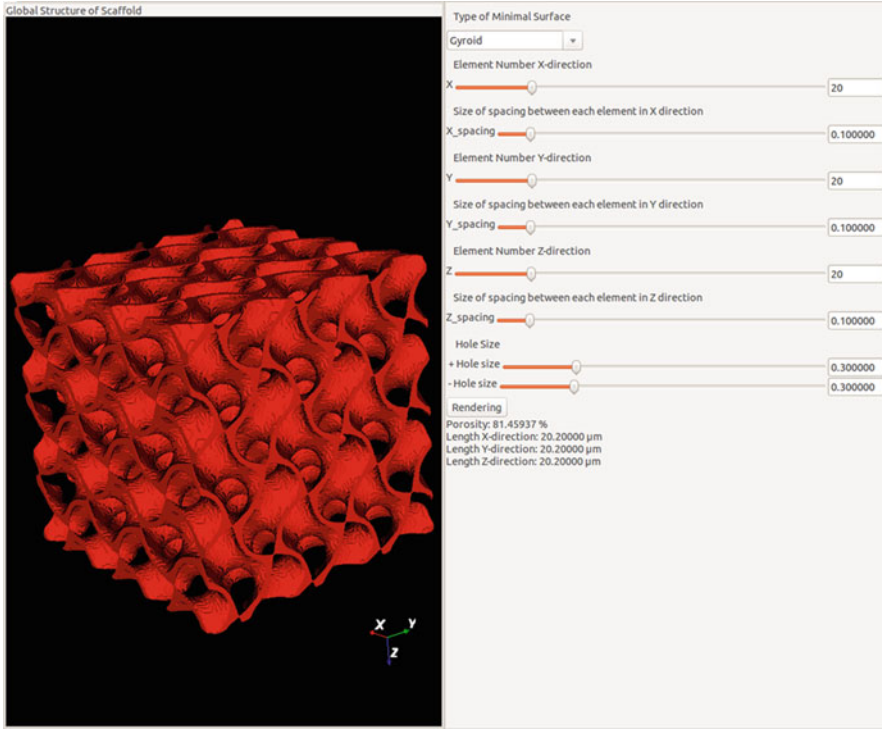


**Fig. 8** Example of the “interface scaffold” developed in Python (Dinis et al. 2014)

where  $r$  is the location vector in the Euclidean space,  $L_k$  is the  $k$  lattice vector in the reciprocal space,  $M_k$  is the magnitude factor,  $\beta_k$  is the wavelength of periods,  $Ps_k$  is the phase shift, and  $C$  is a constant (Wang 2007; Rajagopalan and Robb 2006; Lord and Mackay 2003; Andersson et al. 1988).

In the TPM case, the Weierstrass formula can be used to describe these surfaces in a parametric way (Wang 2007; Rajagopalan and Robb 2006; Lord and Mackay 2003; Andersson et al. 1988):

$$\begin{cases} x = \text{Re} \int_{\omega_0}^{\omega^1} e^{i\theta} (1 - \omega^2) R(\omega) d\omega \\ y = \text{Im} \int_{\omega_0}^{\omega^1} e^{i\theta} (1 + \omega^2) R(\omega) d\omega \\ z = -\text{Re} \int_{\omega_0}^{\omega^1} e^{i\theta} (2\omega^2) R(\omega) d\omega \end{cases} \quad (2)$$

where  $\omega$  is a complex variable,  $\theta$  is the so-called Bonnet angle, and  $R(\omega)$ ,  $Re$ , and  $Im$  are geometric functions varying for different surfaces.

Within the several TPMS models, only the Schwarz Primitive and Schoen I-WP surfaces were considered in this research work (Fig. 10).

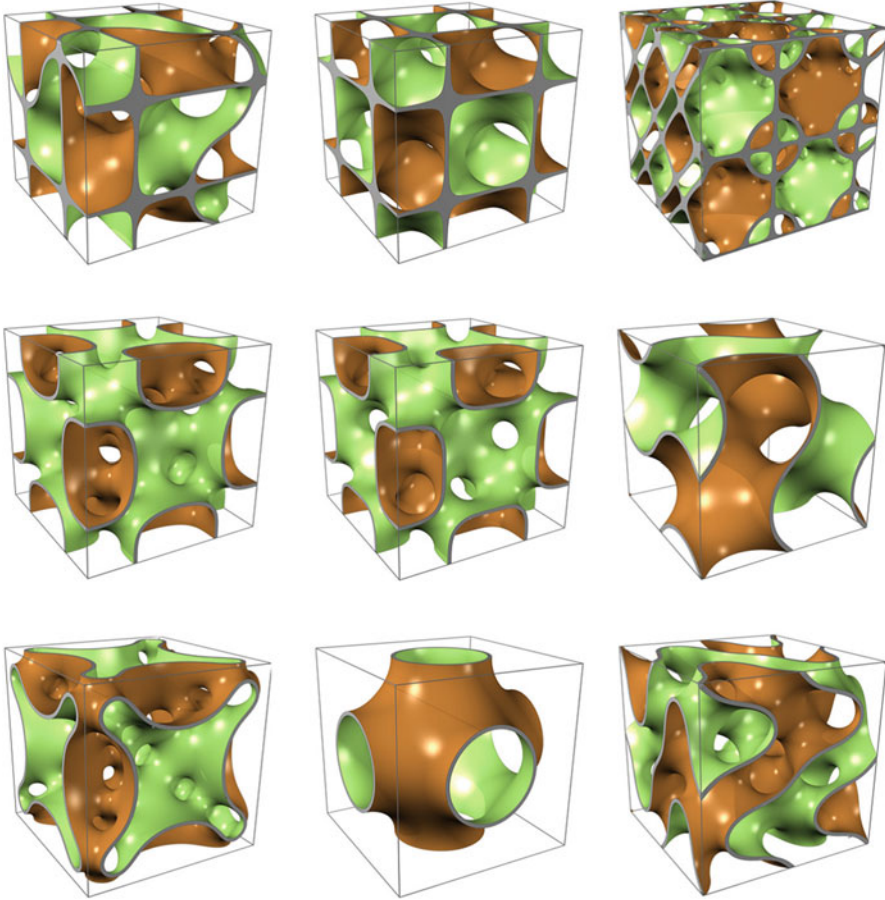


**Fig. 9** Various examples of triply periodic minimal surfaces. From *top left* to *bottom right*, translational unit cells of Fischer Koch Y, Diamond, Disphenoid, Batwing, F-RD, Gyroid, Manta, Schwartz, and Fischer Koch S (Kapfer et al. 2011)

### 3.3 Schwarz TPMS Primitives

A periodic Schwarz Primitive surface can be mathematically described by the following nodal approximation (Wang 2007; Rajagopalan and Robb 2006; Lord and Mackay 2003; Andersson et al. 1988):

$$\phi(r) = M_p \left[ \cos(2\pi x/\beta_x) + \cos(2\pi y/\beta_y) + \cos(2\pi z/\beta_z) \right] \quad (3)$$

Since the previous equation only defines the surface model, the solid geometric modeling of the Schwarz units was obtained using a commercially available CAD software (*Solidworks* from *Dassault Systemes*, [www.3ds.com](http://www.3ds.com)) through offset and thickening operations in order to obtain solid models for production and simulation. Through these operations, the solid geometric modeling enabled to define two

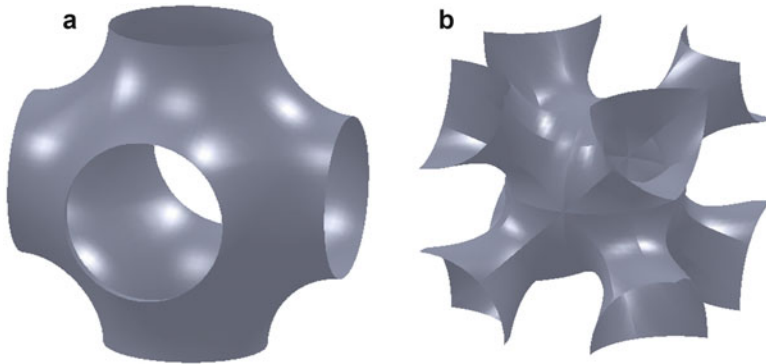


**Fig. 10** (a) Schwarz' Primitive and (b) Schoen I-WP surfaces

important geometric modeling constraint parameters, namely, thickness and radius. Based on these two geometric modeling parameters, two sub-models were defined as follows:

- Thickness variations (the obtained models varied their geometric thickness while maintaining the same geometric radius as illustrated in Fig. 11a and similarly in Fig. 12a)
- Radius variations (the obtained models varied their geometric radius while maintaining the same geometric thickness as illustrated in Fig. 11b and similarly in Fig. 12b).

The variation of these geometric parameters enables changes to the architectural topology of each basic unit of a scaffold, varying its porosity and mechanical and vascular behavior (Fig. 11).

### 3.4 Schoen TPMS Primitives

The mathematical description of a Schoen's I-WP surface is given by the following nodal approximation (Wang 2007; Rajagopalan and Robb 2006; Lord and Mackay 2003; Andersson et al. 1988):

$$\varphi(r) = M_1 \begin{bmatrix} 2 \cos(2\pi x/\beta_x) \cos(2\pi y/\beta_y) + 2 \cos(2\pi y/\beta_y) \cos(2\pi z/\beta_z) \\ 2 \cos(2\pi z/\beta_z) \cos(2\pi x/\beta_x) \\ - \cos(4\pi x/\beta_x) - \cos(4\pi y/\beta_y) + \cos(4\pi z/\beta_z) \end{bmatrix} \quad (4)$$

Similarly to the Schwarz Primitive solid modeling, the solid Schoen units were obtained through the same design offset and thickening operations. By varying the thickness (Fig. 12a) and radius (Fig. 12b) values, different solid geometric models can be obtained as illustrated in Fig. 12.

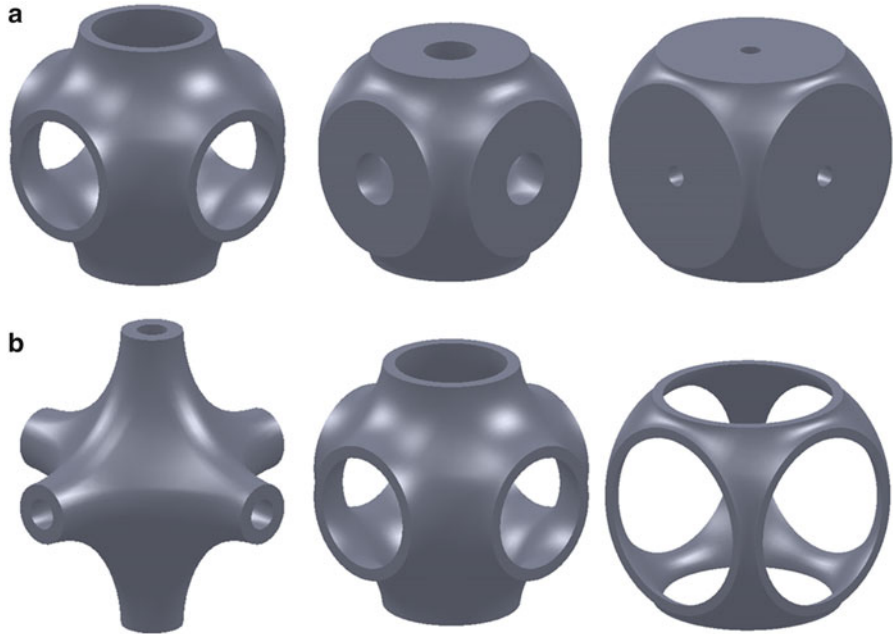


**Fig. 11** Schwarz' Primitive surfaces obtained through (a) surface thickness variation with constant radius and (b) surface radius variation with constant thickness

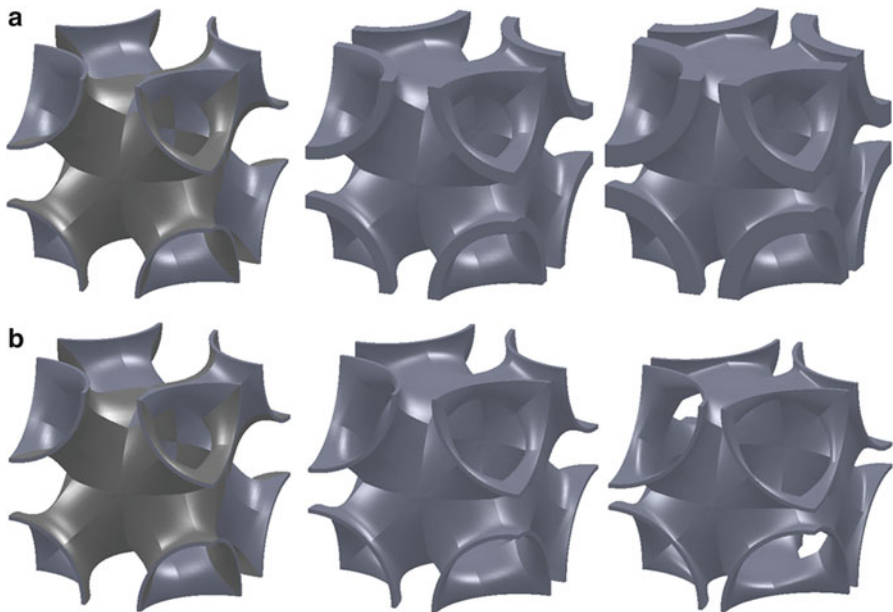


**Fig. 12** Schoen's I-WP surfaces obtained through (a) surface thickness variation with constant radius and (b) surface radius variation with constant thickness

## 4 Numerical Implementation of the Designed Models

The main goal for simulating the scaffold mechanical behavior is to evaluate the porosity dependence on the elastic and shear modulus. The mechanical behavior of these structures is assessed through the finite element method (*Abaqus* from *Dassault Systemes*, [www.3ds.com](http://www.3ds.com)). For a given unit block with a specific open pore architecture, boundary and loading conditions considered for evaluating mechanical properties are shown in Fig. 13:

- For the numerical computation of the elastic modulus (Fig. 13a), a uniform displacement in a single direction is considered (in this case the X direction), which is equivalent to the strain in the same direction ( $\epsilon_x$ ), imposed to a face of the block (Face A). The displacement value is a percentage of displacement ( $Pd_x$ ) equivalent to 0.1% of the unit's block length ( $L_x$ ). The opposite face (Face B) of the scaffold unit is constrained and unable to have any displacement. The average reaction forces ( $Rf_x$ ) produced on Face B of area ( $A_x$ ) are used to determine the elastic modulus (E) (eq. 5) due to the imposed displacement.
- For the numerical computation of the shear modulus (Fig. 13b), a uniform displacement in a single direction is considered (in this case the Y direction), which is equivalent to the strain in the same direction ( $\gamma_{xy}$ ), imposed to a face of the block (Face B). The displacement value is a percentage of displacement ( $Pd_y$ ) equivalent to 0.1% of the unit's block length ( $L_y$ ). The opposite face (Face A) of the scaffold unit is constrained and unable to have any displacement. The two lateral faces (Faces C) are also constrained and unable to have any displacement in the X direction. The average reaction forces ( $Rf_y$ ) produced on Face A of area ( $A_y$ ) is used to determine the shear modulus (G) (Eq. 6) due to the imposed displacement.

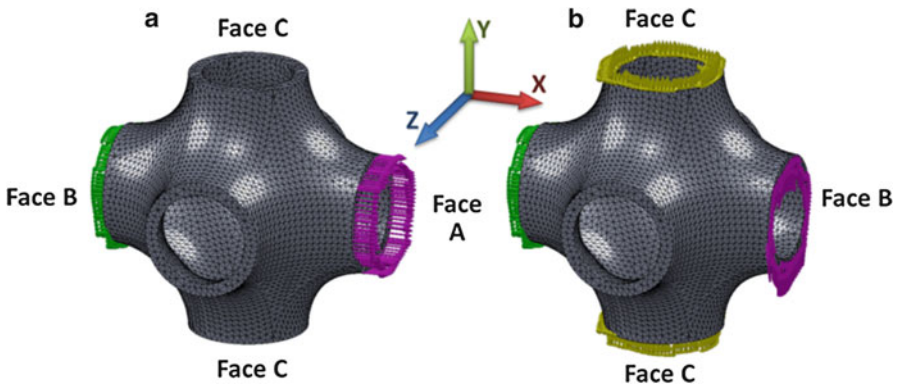


**Fig. 13** Loads and constraints for the numerical analysis of scaffolds under a (a) tensile solicitation and (b) shear solicitation

$$E_{xx} = \frac{\sigma_x}{\epsilon_x} = \frac{\frac{Rf_x}{Pd_x \times L_x} \frac{A_x}{L_x}}{\frac{A_x}{Pd_x}} = Rf_x \quad (5)$$

$$G_{xy} = \frac{\tau_{xy}}{\gamma_{xy}} = \frac{\frac{Rf_x}{Pd_x \times L_y} \frac{A_y}{L_y}}{\frac{A_y}{Pd_x}} = \frac{Rf_x}{Pd_x \times A_y} \quad (6)$$

The material considered for simulation purposes is Poly( $\epsilon$ -caprolactone) (PCL), a semicrystalline biodegradable polymer with a melting point of  $\sim 60$  °C and a glass transition temperature  $\sim -60$  °C. The elastic modulus ( $E_0$ ), shear modulus ( $G_0$ ), and Poisson's ratio of the PCL material considered in the numerical simulations were 400 MPa, 150.38 MPa, and 0.33, respectively (Almeida and Bártolo 2013).

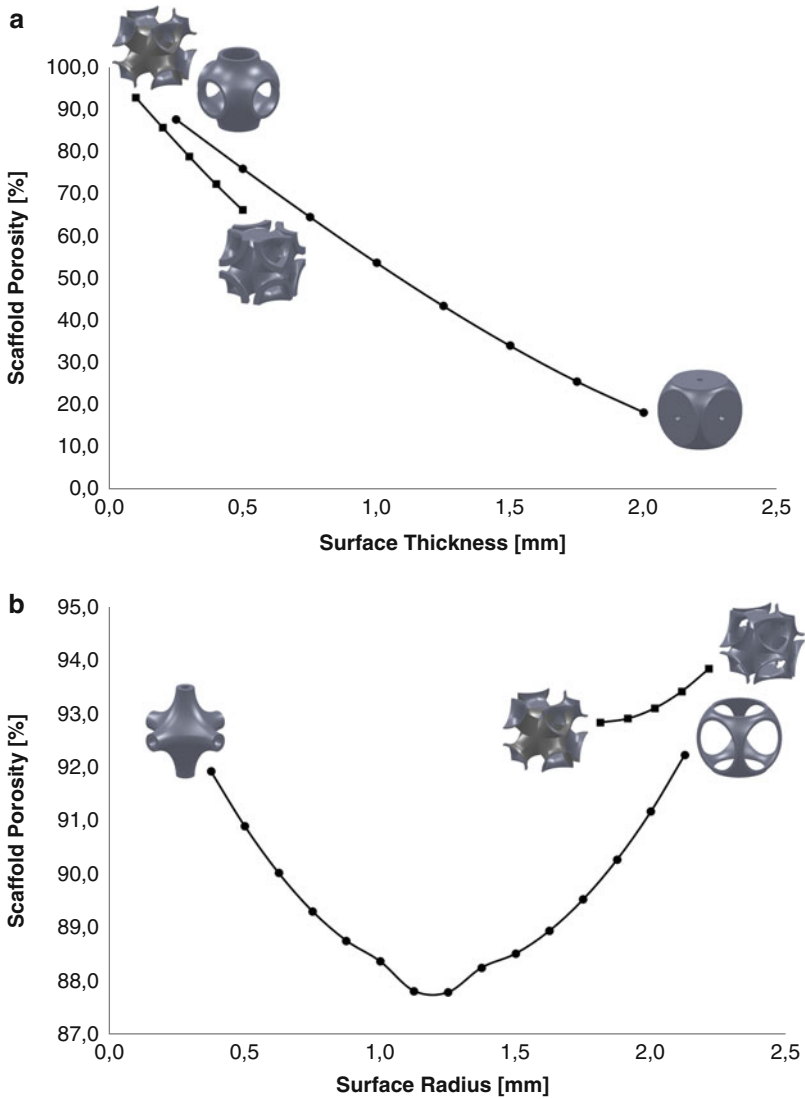
The results will be displayed in function of the scaffold's tensile stress ratio ( $E/E_0$ ) and the scaffold's shear stress ratio ( $G/G_0$ ). The scaffold's tensile stress ratio ( $E/E_0$ ) is determined between the scaffold's tensile modulus ( $E$ ) obtained from the numerical simulations and the material's tensile reference modulus ( $E_0$ ). Similarly, the scaffold's shear stress ratio ( $G/G_0$ ) is determined between the scaffold's shear modulus ( $G$ ) obtained from the numerical simulations and the material's tensile reference modulus ( $G_0$ ). Figures 14, 15, 16, 18, and 19 contain two charts with two data curves each, whereas each data curve corresponds to either the Schwarz Primitive or the Schoen I-WP surfaces. Accompanying each data curve, there are two figures associated with the type of corresponding TPMS and its geometric variation.

The variation of the scaffold's porosity as a function of surface thickness and surface radius for both Schwarz' Primitives and Schoen's I-WP surfaces are presented in Fig. 14. Results show that the porosity decreases with the increasing of surface thickness (Figs. 14a).

Regarding the surface radius for the Schwarz Primitive surfaces, it is possible to observe its effect on the porosity (Fig. 14b). The porosity tends to decrease with increasing surface radius till a threshold value, from which it starts to increase. In this case, the relationship between porosity and surface radius has a hyperbolic behavior. In the case of the Schoen I-WP surfaces, the effect of changing the surface radius, as illustrated in Fig. 14b, shows that the porosity increases with increasing surface radius.

## 4.1 Elastic Modulus Evaluation

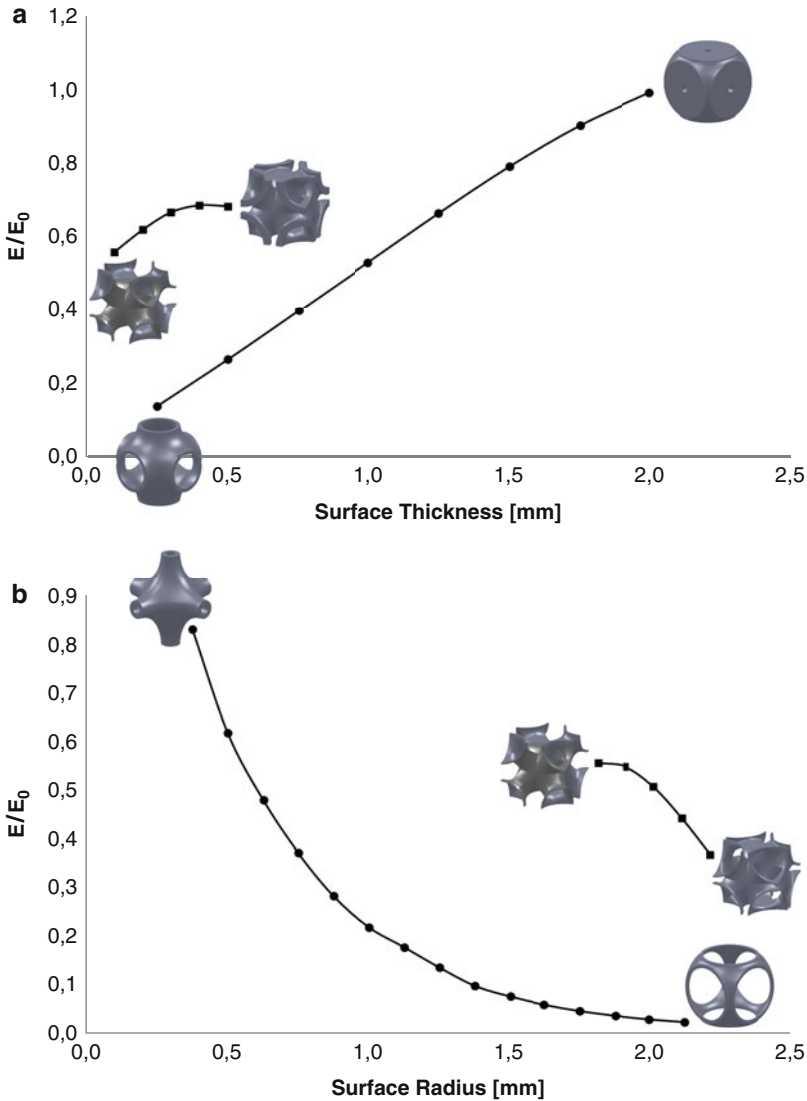
The variation of the elastic modulus as a function of surface thickness and surface radius for both Schwarz' Primitives and Schoen's I-WP surfaces are presented in Fig. 15. Results show that the elastic modulus tends to increase with the increase of



**Fig. 14** Variation of the scaffold’s porosity with the (a) surface thickness and (b) surface radius for both geometries

surface thickness, for both geometric surfaces (Fig. 15a). Regarding the influence of the surface radius in both TPMS models, as the surface radius increases, the elastic modulus tends to decrease in a nonlinear way, as illustrated in Fig. 15b).

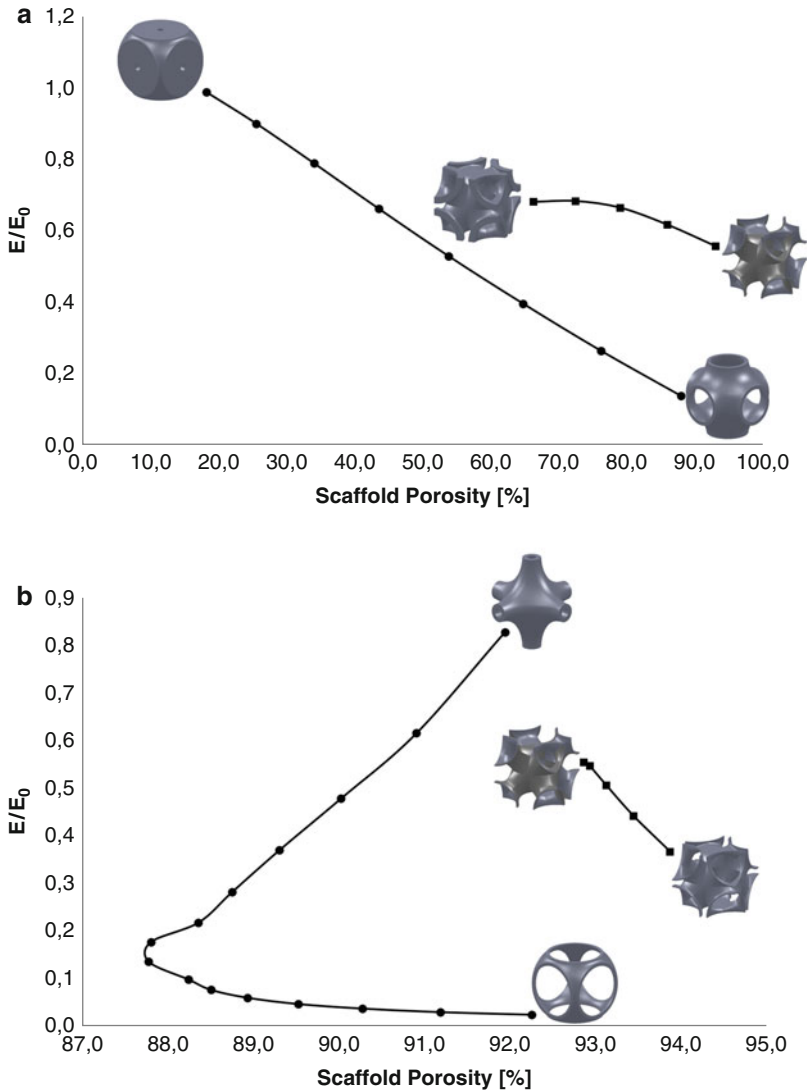
Figure 16 illustrates the variation of the elastic modulus of both TPMS models based on the variation of the surface thickness (Fig. 16a) and surface radius (Fig. 16b).



**Fig. 15** Variation of the scaffold’s elastic modulus with the (a) surface thickness and (b) surface radius for both geometries

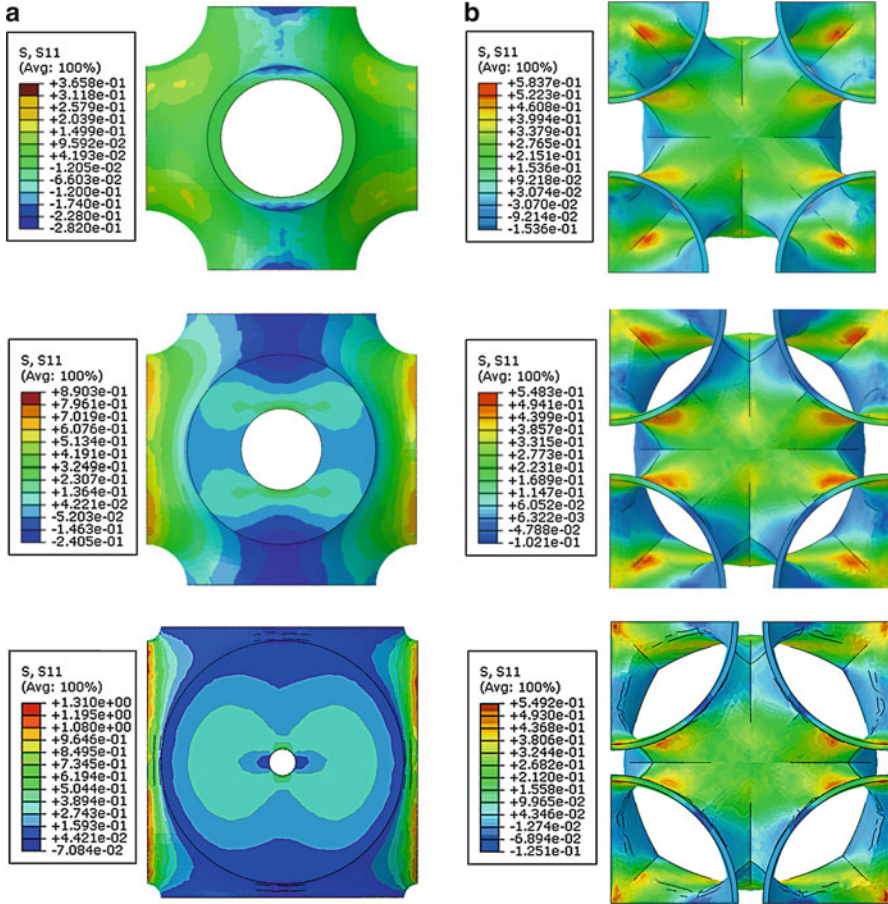
Regarding the thickness variation, both models present an almost linear dependence between the scaffold’s porosity and the elastic modulus. In both TPMS models, the elastic modulus decreases with the increasing surface thickness (Fig. 16a).

Regarding the surface radius, a similar hyperbolic behavior was observed for the Schwarz Primitive surfaces between the elastic modulus and porosity (Fig. 16b), so



**Fig. 16** Variation of the scaffold’s elastic modulus as a function of porosity with the (a) surface thickness and (b) surface radius for both geometries

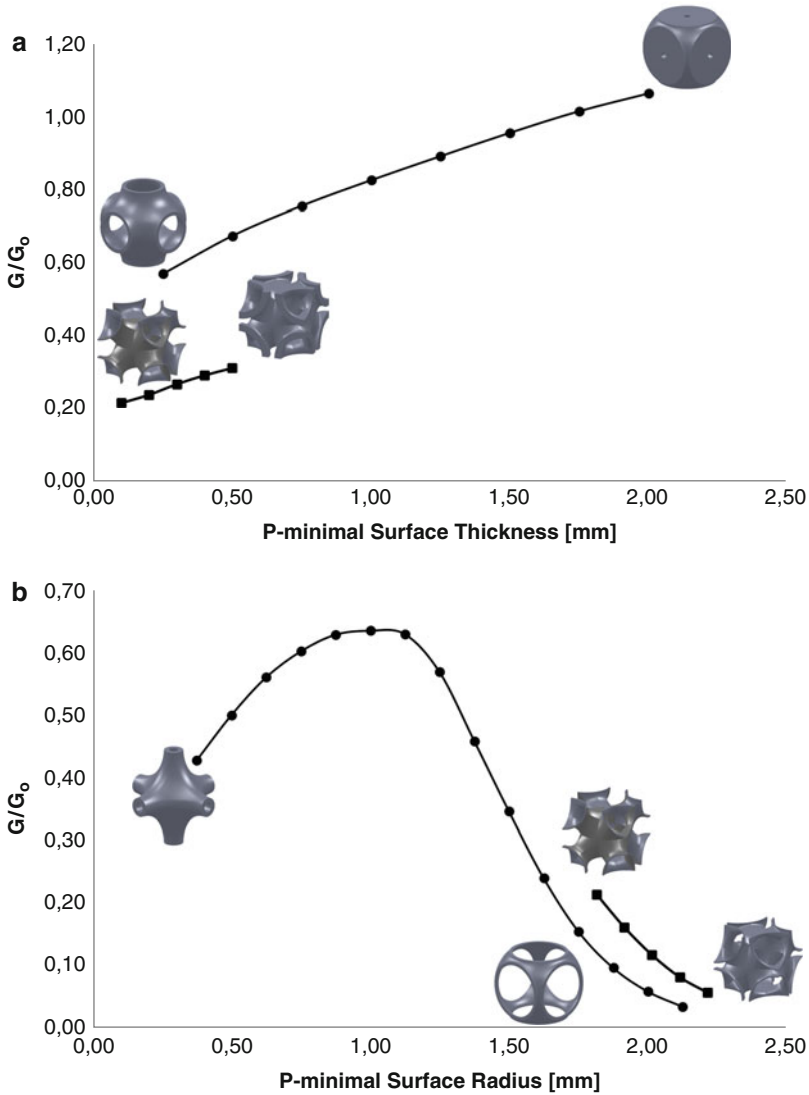
we may decrease or increase the elastic modulus of the scaffold while maintaining high porosity values, which offers great flexibility regarding scaffold design. High porosity is critical for vascularization and tissue ingrowth. In the case of Schoen’s I-WP surfaces, the elastic modulus tends to increase with the increase of porosity (Fig. 16b).



**Fig. 17** Variation of the scaffold's tensile stress for (a) Schwarz' Primitive surface with surface thickness and (b) Schoen's I-WP surface with surface radius

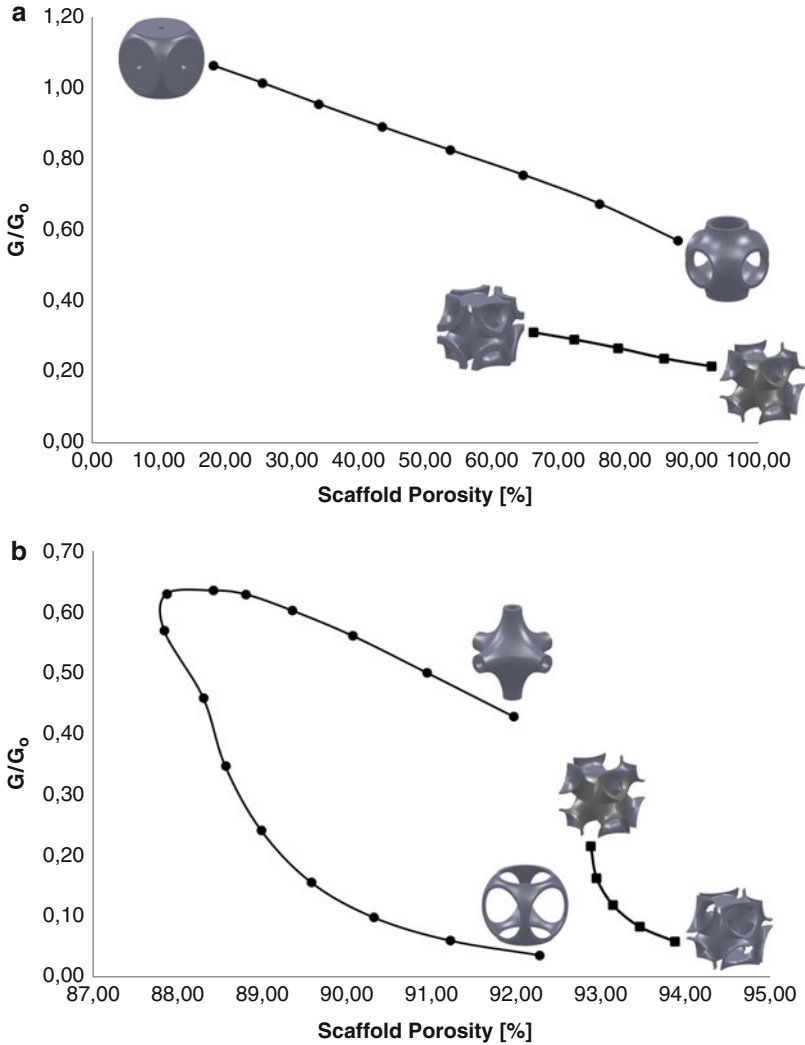
Figures 15 and 16 illustrate the scaffold's basic unit mechanical behavior on a macroscale level regarding geometric parameters, such as radius and thickness, for both Schwarz' Primitive and Schoen's I-WP surfaces. Figure 17 illustrates the tensile stress variation of the scaffold on a microscale level, considering the variation of both the thickness (Fig. 17a) for the Schwarz Primitive geometry and the radius for the Schoen I-WP (Fig. 17b)).

Figure 17a shows that by increasing the thickness in the Schwarz Primitive geometries, the tensile stresses tend to assume lower values at the two lateral faces, resulting in an uneven tensile stress distribution. The scaffold presents a more homogenous tensile distribution for lower thickness values. Regarding the radius variation, there is no significant tensile stress variation with the radius increase.



**Fig. 18** Variation of the scaffold’s shear modulus with the (a) surface thickness and (b) surface radius for both geometries

A similar behavior is observed for the Schoen I-WP thickness variation. The Schoen geometries present a more homogenous tensile stress for lower thickness values. Regarding the radius variation (Fig. 17b), results show that, as the radius increases, a more differentiated tensile stress distribution is observed, namely, in the central sphere of the Schoen geometry. In this case, Schoen geometries with lower radius values present a more homogenous tensile distribution for cell differentiation and proliferation.



**Fig. 19** Variation of the scaffold shear modulus as a function of porosity with the (a) surface thickness and (b) surface radius for both geometries

### 4.2 Shear Modulus Evaluation

Figure 18a shows that the shear modulus ratio increases with thickness. This figure also demonstrates that the Schwarz Primitive surface presents a higher shear modulus behavior compared to the material's reference shear modulus. In other words, the Schwarz Primitive surface increases the shear performance above reference for high thickness values. For the Schoen I-WP surface, Fig. 18a shows that the shear modulus ratio increases with thickness. Regarding the effect of the Schwarz

Primitive surface radius variations, Fig. 18b shows that the shear modulus ratio increases and then begins to decrease as the Schwarz Primitive surface radius increases. Regarding the Schoen I-WP surface, the shear modulus ratio decreases by increasing the surface radius (Fig. 18b).

A linear dependence between the scaffold porosity and the shear modulus ratio was obtained as observed in Fig. 19a. For the Schoen I-WP surface, Fig. 19a shows that the shear modulus ratio decreases with porosity. In spite of the porosity and the radius having a hyperbolic behavior, the shear modulus ratio with the Schwarz Primitive surface radius has a sinusoidal behavior, while the shear modulus ratio with the porosity has an approximated hyperbolic behavior (Fig. 19b). In this case, we may decrease or increase the shear modulus of the scaffold while maintaining high porosity values. Regarding the Schoen I-WP surface, the shear modulus ratio decreases by increasing the porosity (Fig. 19b).

Figures 18 and 19 illustrate the scaffold's basic unit mechanical behavior on a macroscale level regarding geometric parameters, such as radius and thickness, for both the Schwarz Primitive and Schoen I-WP surfaces. Figure 20 illustrates the shear stress variation of the scaffold on a microscale level, considering the variation of both the thickness (Fig. 20a) for the Schwarz Primitive geometry and the radius for the Schoen I-WP (Fig. 20b).

Figure 20a shows that by increasing the thickness in the Schwarz Primitive geometries, the shear stresses tend to assume lower values at the two lateral faces that present either no constraint or solicitation, resulting in an uneven shear stress distribution. The scaffold presents a more homogenous tensile distribution for lower thickness values. Regarding the radius variation, there is no significant shear stress variation with the radius increase.

A similar behavior is observed for the Schoen I-WP thickness variation. The Schoen I-WP geometries present a more homogenous shear stress for lower thickness values. Regarding the radius variation (Fig. 20b), results show that, as the radius increases, a more differentiated shear stress distribution is observed, namely, in the central sphere of the Schoen geometry. In this case, Schoen's I-WP geometries with higher radius values present a more homogenous shear distribution for cell differentiation and proliferation.

---

## 5 Design of a Functionally Gradient Scaffold Using TPMS Basic Units

Figure 21 illustrates the Boolean operations by the addition of the repeating units into an arbitrary unit with thickness variation, resulting in a scaffold with a thickness gradient. Figure 22 illustrates the production of both scaffolds in ABSPlus material through an extrusion-based additive manufacturing system, called the uPrint SE 3D Printer from Stratasys.

Structural simulations were performed on the combined model, including several the Schwarz Primitive and Schoen I-WP elementary scaffold units with a thickness gradient. A displacement solicitation along the direction of the thickness gradient

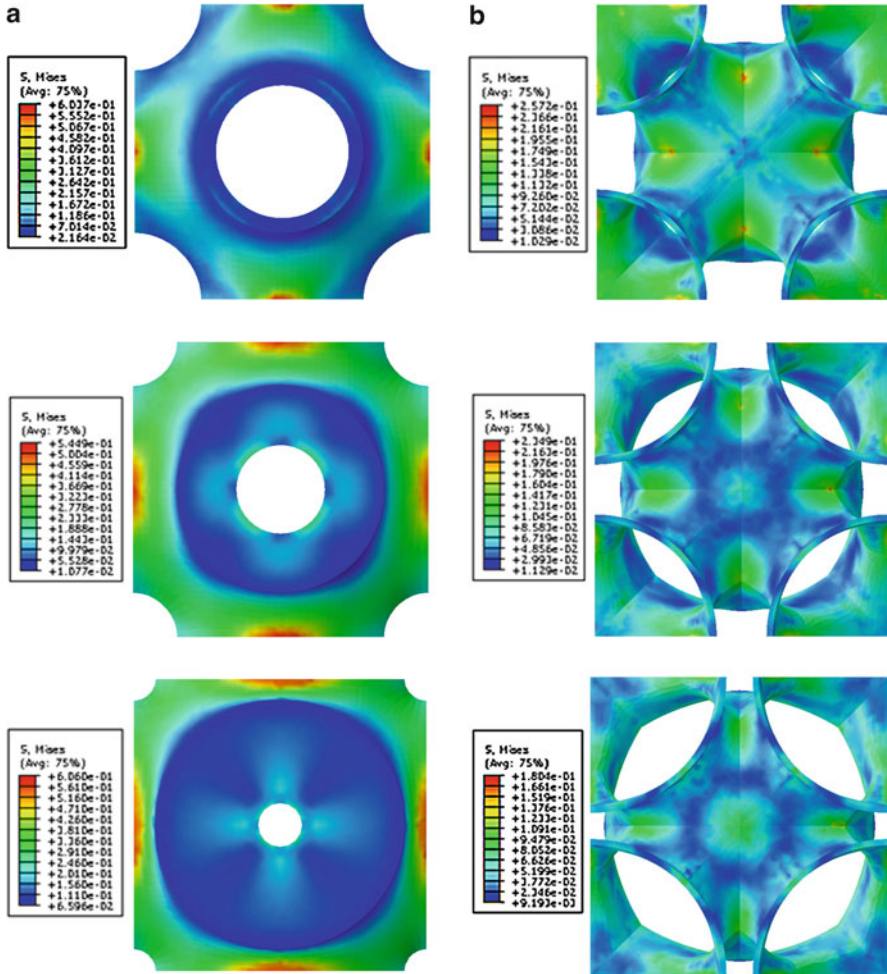


**Fig. 20** Variation of the scaffold's shear stress for the (a) Schwarz Primitive surface with surface thickness and (b) Schoen I-WP surface with surface radius

was defined, in order to undergo the simulations. For both scaffold models, results show that as the thickness of the elementary units increase, the tensile variations tend to lower in value and become more homogenous, as illustrated in Fig. 23.

## 6 Conclusions

The design of optimized scaffolds for tissue engineering applications is a key topic of research, as the complex macro- and micro-architectures required for a scaffold depends on the mechanical and vascular properties and physical and molecular

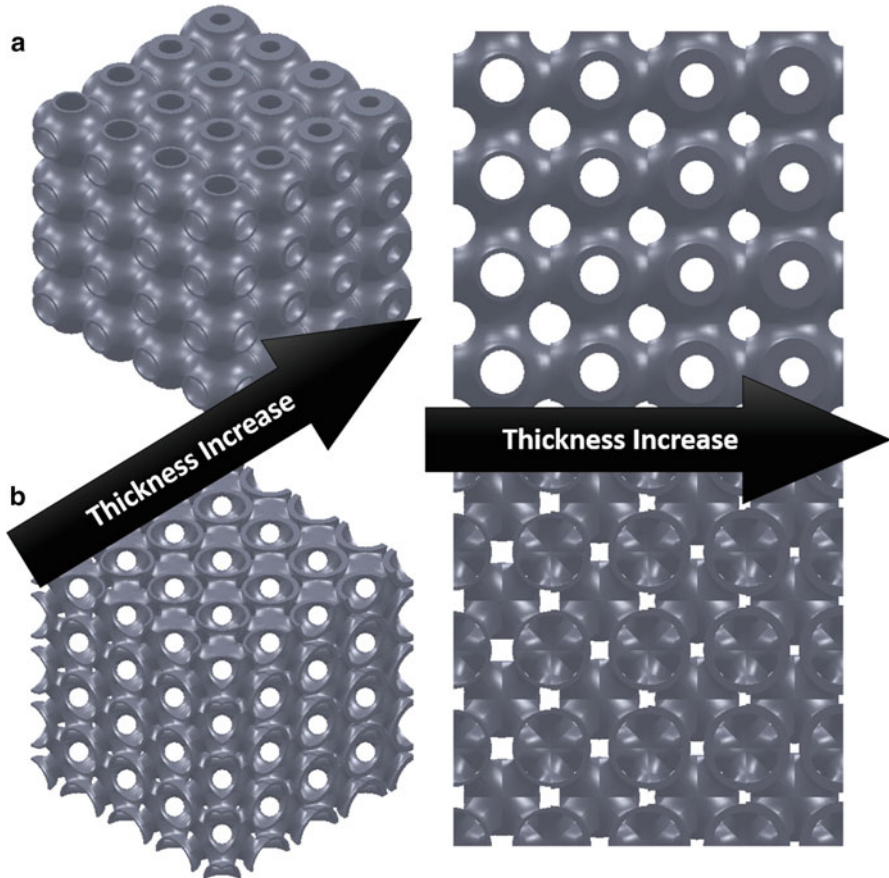


**Fig. 21** CAD models illustrating thickness gradient within the scaffold structures for the (a) Schwarz Primitive and (b) Schoen I-WP geometries

queues of the surrounding tissue at the defect site. One way to achieve such hierarchical designs is to create a library of unit cells which can be assembled through a computational tool. Several scaffold design methodologies were presented. The initial designs contemplated regular geometric designs, either based on geometric designs (struts, spheres, beams, rods, etc.), medical images, or homogenization theories. Recently, periodic surface modeling was implemented into the scaffold design process, presenting higher mechanical, vascular, and biological performance in tissue engineering applications.

Understanding the mechanical properties of highly porous scaffolds, from the knowledge of its microstructure, is a topical research area in tissue engineering. In this work, porous scaffolds were designed, and its mechanical behavior was simulated using triply periodic minimal surfaces, namely, Schwarz and Schoen geometries. These geometries allow the design of highly porous structures with optimum mechanical and vascular properties.

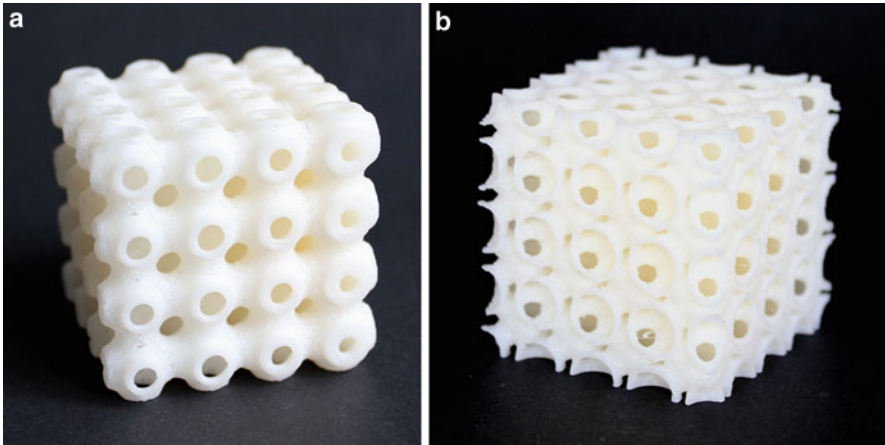


**Fig. 22** Physical models of (a) the Schwarz Primitive and (b) Schoen I-WP geometries produced through extrusion-based additive manufacturing

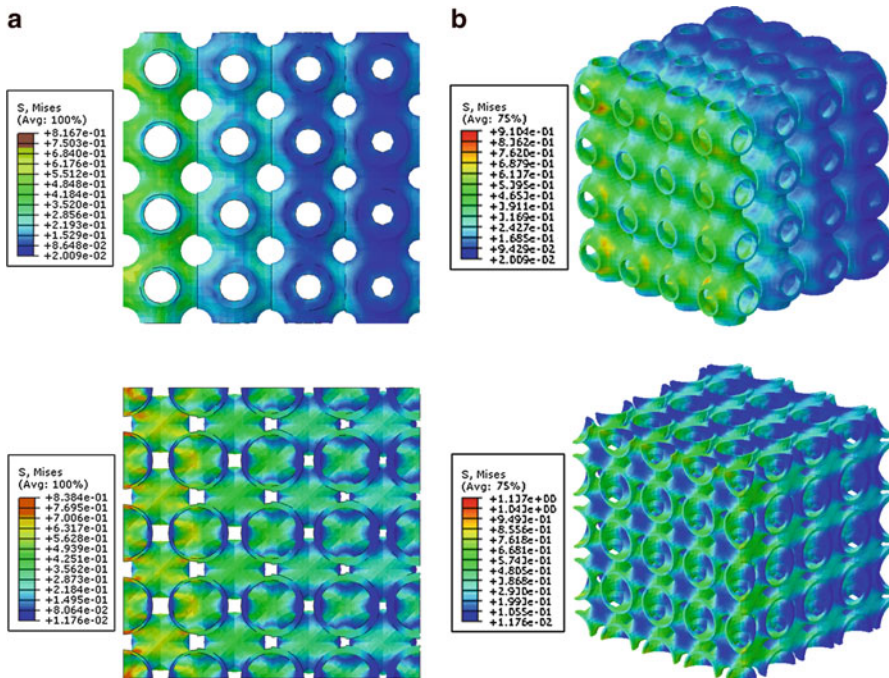


**Fig. 23** Variation of the Tensile Stress along the thickness gradient for both scaffold structures for the (a) Schwarz Primitive and (b) Schoen I-WP geometries

Based on the tensile simulations, both geometries, results show that an increase in the surface thickness implies both a decrease in the porosity and improved mechanical performance. Nevertheless, as the thickness increases, and despite an

increase in the mechanical properties, the tensile stress distribution of the geometries becomes less homogenous inside the models.

Results also show that, for Schoen's I-WP surfaces, the increase of the surface radius increases the porosity and decreases the mechanical performance. The Schoen I-WP surfaces also have less optimum mechanical distributions as the radius increases. In the case of the Schwarz geometries, as the radius increases, the porosity tends to decrease until a certain threshold value, after which it starts to increase again (parabolic behavior). The mechanical performance decreases with the radius increase. A parabolic behavior is also observed for the mechanical performance, as a function of the porosity for the Schwarz geometries.

Based on the shear simulations, the Schwarz geometries, the results show that porosity decreases with the P-minimal surface thickness, decreasing also till a threshold value for the P-minimal surface radius. From this threshold value, the porosity then starts to increase. The shear modulus ratio increases with the P-minimal surface thickness and presents an approximated hyperbolic behavior by increasing the P-minimal surface radius.

Regarding the Schoen geometries, the results show that porosity decreases and the shear modulus ratio increases with the P-minimal surface thickness. On the other hand, the porosity increases and the shear modulus decreases with the P-minimal surface radius. In both cases, the shear modulus ratio decreases with the porosity.

When comparing both geometries, concerning the thickness variation, Schoen geometries present both lower values of porosity and lower values of shear modulus ratio. Regarding the radius variations, Schoen geometries present slightly higher porosity levels but still lower values of shear modulus ratio when compared to the Schwarz geometries. Schwarz geometries present a more versatile behavior, for one given porosity, you may have a structure with a lower or higher shear modulus, and they also present a higher range of values for both shear modulus ratio and porosity levels, when compared to Schoen geometries.

Minimal surfaces (surfaces of zero mean curvature or an average negative Gaussian curve) enable the design of smooth biomorphic constructs, providing an optimal biomechanical environment for cell attachment, migration, and proliferation, enabling optimization of the relationship between surface area, porosity, and mechanical properties. By using triply periodic surfaces in scaffold design for tissue engineering applications, it is possible to use highly porous structures with optimum mechanical properties. Several of the previous works performed by Yoo presented design schemes on how to developed bone scaffold implants, but by associating the mechanical behavior, it is possible to optimize the designs and produce bone scaffolds as a function of both geometric design and mechanical performance.

---

## References

- Almeida, H.A. and Bártolo, P.J. (2008) computer simulation and optimisation of tissue engineering scaffolds: mechanical and vascular behaviour", 9th biennial ASME conference on engineering systems design and analysis (ESDA2008), Y. Halevi and A. Fischer (Eds.), ASME conference proceedings, Haifa Isreal.

- Almeida HA, Bártolo PJ (2012a) Chapter 12: Structural and vascular analysis of tissue engineering scaffolds: part 1 – numerical fluid analysis. In: Liebschner M, Kim D (eds) *Computer-aided tissue engineering*. Springer, London
- Almeida HA, Bártolo PJ (2012b) Chapter 13: Structural and vascular analysis of tissue engineering scaffolds: part 2 – topology optimization. In: Liebschner M, Kim D (eds) *computer-aided tissue engineering*. Springer, London
- Almeida HA, Bártolo PJ (2013) Numerical simulations of BioExtruded polymer scaffolds for tissue engineering applications. *Polym Int* 62(11):1544–1552
- Almeida HA, Bártolo PJ, Ferreira J (2007a) Mechanical behaviour and vascularisation analysis of tissue engineering scaffolds. In: Bártolo PJ et al (eds) *Virtual and rapid manufacturing – Advanced research in virtual and rapid prototyping*. Taylor & Francis, London, pp 73–80
- Almeida HA, Bártolo PJ, Ferreira J (2007b) Design of scaffolds assisted by computer. In: Brebbia CA (ed) *Modelling in medicine and biology VII*. Wit Press, pp 157–166
- Andersson S (1983) On the description of complex inorganic crystal structures. *Angew Chem Int Ed* 22(2):69–81
- Andersson S, Hyde ST, Larsson K, Lidin S (1988) Minimal surfaces and structures: from inorganic and metal crystals to cell membranes and biopolymers. *Chem Rev* 88:221–242
- Bao G, Suresh S (2003) Cell and molecular mechanics of biological materials. *Nature Materials* 2:715–725
- Bártolo PJ, Almeida HA, Rezende RA, Laoui T, Bidanda B (2008) Advanced processes to fabricate scaffolds for tissue engineering. In: Bidanda B, Bártolo PJ (eds) *Virtual Prototyping & bio-Manufacturing in medical applications*. Springer, New York, pp 151–174
- Bártolo PJ, Almeida H, Laoui T (2009a) Rapid prototyping & manufacturing for tissue engineering scaffolds. *Int J Comput Appl Technol* 36(1):1–9
- Bártolo PJ, Chua CK, Almeida HA, Chou SM, Lim ASC (2009b) Biomanufacturing for tissue engineering: present and future trends. *Virtual Phys Prototyping* 4(4):203–216
- Bártolo PJ, Kruth JP, Silva J, Levy G, Malshe A, Rajurkar K, Mitsuishi M, Ciurana J, Leu M (2012) Biomedical production of implants by additive electro-chemical and physical processes. *CIRP Ann Manuf Technol* 61(2):635–655
- Brunello G, Sivolella S, Meneghello R, Ferroni L, Gardin C, Piattelli A, Zavan B, Bressan E (2016) Powder-based 3D printing for bone tissue engineering. *Biotechnol Adv* 34:740–753
- Dinis JC, Morais TF, Amorin PHJ, Ruben RB, Almeida HA, Inforçati PN, Bártolo PJ, Silva JVL (2014) Open source software for the automatic Design of Scaffold Structures for tissue engineering applications. *Procedia Technol* 16:1542–1547
- Eshraghi S, Das S (2010) Mechanical and microstructural properties of polycaprolactonescaffolds with one-dimensional, two-dimensional, and three-dimensional orthogonally oriented porous architectures produced by selective laser sintering. *Acta Biomater* 6(7):2467–2476
- Fallahiarezoudar E, Ahmadipourrouposht M, Idris A, Yusof NM (2015) A review of: application of synthetic scaffold in tissue engineering heart valves. *Mater Sci Eng C* 48:556–565
- Gandy PJF, Bardhan S, Mackay AL, Klinowski J (2001) Nodal surface approximations to the P, G, D and I-WP triply periodic minimal surfaces. *Chem Phys Lett* 336(3):187–195
- Giannitelli SM, Mozetic P, Trombetta M, Rainer A (2015) Combined additive manufacturing approaches in tissue engineering. *Acta Biomater* 24:1–11
- Gibson LJ (2005) Biomechanics of cellular solids. *J Biomech* 38:377–399
- Hyde S (1996) Bicontinuous structures in lyotropic liquid crystals and crystalline hyperbolic surfaces. *Curr Opin Solid State Mater Sci* 1:653–662
- Hyde ST, Oguey C (2000) From 2D hyperbolic forests to 3D Euclidean entangled thickets. *Eur Phys J B* 16(4):613–630
- Jana S, Lerman A (2015) Bioprinting a cardiac valve. *Biotechnol Adv* 33:1503–1521
- Janik H, Marzec M (2015) A review: fabrication of porous polyurethane scaffolds. *Mater Sci Eng C* 48:586–591

- Jazayeri HE, Tahriri M, Razavi M, Khoshroo K, Fahimipour F, Dashtimoghadam E, Almeida L, Tayebi L (2017) A current overview of materials and strategies for potential use in maxillofacial tissue regeneration. *Mater Sci Eng C* 70:913–929
- Jiang T, Carbone EJ, Lo KWH, Laurencin CT (2015) Electrospinning of polymer nanofibers for tissue regeneration. *Prog Polym Sci* 46:1–24
- Jung Y, Chu KT, Torquato S (2007) A variational level set approach for surface area minimization of triply-periodic surfaces. *J Comput Phys* 223(2):711–730
- Kapfer SC, Hyde ST, Mecke K, Arns CH, Schroder-Turk GE (2011) Minimal surface scaffold designs for tissue engineering. *Biomaterials* 32(29):6875–6882
- Karcher H, Polthier K (2014) Construction of triply periodic minimal surfaces. *Philos Trans R Soc Lond A* 354(1715):2077–2104
- Langer R, Vacanti JP (1993) Tissue engineering. *Science* 260:920–926
- Larsson M, Terasaki O, Larsson K (2003) A solid state transition in the tetragonal lipid bilayer structure at the lung alveolar surface. *Solid State Sci* 5(1):109–114
- Law JX, Liau LL, Aminuddin BS, Ruszymah BHI (2016) Tissue-engineered trachea: a review. *Int J Pediatr Otorhinolaryngol* 91:55–63
- Lord EA, Mackay AL (2003) Periodic minimal surfaces of cubic symmetry. *Curr Sci* 85(3):346–362
- Melchels FPW, Barradas AMC, Blitterswijk CA, Boer J, Feijen J (2010a) Effects of the architecture of tissue engineering scaffolds on cell seeding and culturing. *Acta Biomater* 6(11):4208–4217
- Melchels FPW, Bertoldi K, Gabbelli R, Velders AH, Feijen J (2010b) Mathematically defined tissue engineering scaffold architectures prepared by stereolithography. *Biomaterials* 31(27):6909–6916
- Melek LN (2015) Tissue engineering in oral and maxillofacial reconstruction. *Tanta Dent J* 12:211–223
- Nesper R, Leoni S (2001) On tilings and patterns on hyperbolic surfaces and their relation to structural chemistry. *ChemPhysChem* 2(7):413–422
- Osman NI, Hillary C, Bullock AJ, MacNeil S, Chapple CR (2015) Tissue engineered buccal mucosa for urethroplasty: progress and future directions. *Adv Drug Deliv Rev* 82–83:69–76
- Qi C, Wang Y (2009) Feature-based crystal construction in computer-aided nano-design. *Comput Aided Des* 41(11):792–800
- Rajagopalan S, Robb RA (2006) Schwarz meets Schwann: design and fabrication of biomorphic and durataxic tissue engineering scaffolds. *Med Image Anal* 10(5):693–712
- Risbud M (2001) Tissue engineering: implications in the treatment of organ and tissue defects. *Biogerontology* 2:117–125
- Scriven LE (1976) Equilibrium bicontinuous structure. *Nature* 263(5573):123–125
- Selimis A, Mironov V, Farsari M (2015) Direct laser writing: principles and materials for scaffold 3D printing. *Microelectron Eng* 132:83–89
- Skalak R, Fox CF (1988) *Tissue Engineering*. Alan R. Liss, New York
- Stratton, S., Shelke, N.B., Hoshino, K., Rudraiah, S. and Kumber S.G. (2016) “Bioactive polymeric scaffolds for tissue engineering”, *Bioact Mater*, 1:93–108.
- Sun W, Lal P (2002) Recent development on computer aided tissue engineering - a review. *Comput Methods Prog Biomed* 67:85–103
- Tajbakhsh S, Hajiali F (2017) A comprehensive study on the fabrication and properties of biocomposites of poly(lactic acid)/ceramics for bone tissue engineering. *Mater Sci Eng C* 70:897–912
- Tan KH, Chua CK, Leong KF, Cheah CM, Gui WS, Tan WS, Wiria FE (2005) Selective laser sintering of biocompatible polymers for applications in tissue engineering. *Biomed Mater Eng* 15:113–124
- Tollema V, Collier ZJ, Mohammed MK, Lee MJ, Ameer GA, Reid RR (2016) Stem cells, growth factors and scaffolds in craniofacial regenerative medicine. *Genes Dis* 3:56–71
- Vozzi G, Flaim C, Ahluwalia A, Bhatia S (2003) Fabrication of PLGA scaffolds using soft lithography and microsyringe deposition. *Biomaterials* 24:2533–2540
- Wang Y (2007) Periodic surface modeling for computer aided nano design. *Comput Aided Des* 39(3):179–189

- Xue Y, Sant V, Phillippi J, Sant S (2017) Biodegradable and biomimetic elastomeric scaffolds for tissue engineered heart valves. *Acta Biomater* 48:2–19
- Yoo DJ (2011a) Computer-aided porous scaffold design for tissue engineering using triply periodic minimal surfaces. *Int J Precis Eng Manuf* 12(1):61–71
- Yoo DJ (2011b) Porous scaffold design using the distance field and triply periodic minimal surface models. *Biomaterials* 32(31):7741–7754
- Yoo DJ (2012a) Heterogeneous porous scaffold design for tissue engineering using triply periodic minimal surfaces. *Int J Precis Eng Manuf* 13(4):527–537
- Yoo, D.J. (2012b) Heterogeneous minimal surface porous scaffold design using the distance field and radial basis functions, *Med Eng Phys* 34(5):625–639
- Yoo DJ (2013) Heterogeneous porous scaffold design using the continuous transformations of triply periodic minimal surface models. *Int J Precis Eng Manuf* 14(10):1743–1753
- Yoo DJ (2014) Advanced porous scaffold design using multi-void triply periodic minimal surface models with high surface area to volume ratios. *Int J Precis Eng Manuf* 15(8):1657–1666